15th International Symposium on Ballistics

Jerusalem, Israel, 21 - 24 May, 1995

TUNGSTEN CARBIDE FRAGMENTATION: EXPERIMENTAL CHARACTERIZATION AND NUMERICAL MODELLING

E. S. Hertel, Jr. and D. E. Grady
Sandia National Laboratories
P. O. Box 5800
Albuquerque, New Mexico 87185-0819

Tungsten Carbide is a high density ceramic (generally found in ceramic/metal mixtures) with attractive shear and tensile strength properties in certain ballistic applications. We have determined a Hugoniot elastic limit of ~4 GPa, followed by strong hardening behavior, with spall strengths of 2.7-3.6 GPa. In addition, a series of experiments where Tungsten Carbide spheres impacted PMMA indicates that a sharp transition to fine-grained fragmentation occurred at impact velocities between 2.4 and 2.9 km/s. The well-characterized experiments described above were used to assess the effectiveness of CTH in predicting the axial and radial dispersion of the projectile after break-up. CTH has a fracture model that relies on a P_{min} criteria to allow computational void to relieve a tensile condition. Comparisons with the experimental data were made using the P_{min} model and an additional model based on an energy-based theory of Grady and Kipp. We found that the simple models are not capable of predicting the complex fragmentation behavior seen in the experiments.

INTRODUCTION

Tungsten Carbide is a high density ceramic with attractive shear and tensile strength properties in certain ballistic applications. The current study was undertaken in part to investigate the dynamic equation of state, strength, and fragmentation properties of Tungsten Carbide for the purpose of supporting computational modelling under high velocity impact. Unique Hugoniot elastic limit, release wave, and fragmentation characteristics were observed in our work. The data acquired was used for a series of validation simulations with the multi-dimensional shock physics analysis package, CTH [1]. The principal interest was in applying the capabilities of Eulerian codes in predicting the complex fragmentation phenomena seen when hard, brittle projectiles impact at velocities high enough to cause break-up of the projectile. A series of well-characterized experiments was used to assess the effectiveness of CTH in predicting the axial and radial dispersion of the projectile after break-up. Current modelling capabilities in CTH are typical of those in Eulerian shock physics codes. CTH has a model that relies on a P_{min} criteria to allow computational void to relieve a tensile condition. This model is appropriate for hydrodynamic spall phenomena and has been widely applied to complex problems. Comparisons with our experimental data were made using the P_{min} model and an additional model founded on an energy-based fragmentation theory of Grady and Kipp [2]. We found that

the simple P_{min} model is not capable of predicting the complex fragmentation behavior seen in these experiments but the model based on Grady-Kipp was. A critical issue in modelling the dynamic failure of solids is a need for material property data which characterize the failure and fragmentation behavior under intense stress-wave loading. Although static fracture data frequently exist for these materials, the current state of theoretical understanding does not provide for the confident extension of these data into the highly dynamic regime.

EXPERIMENTAL DATA AND METHODS

Two Tungsten Carbides prepared by pressureless liquid-phase sintering were tested in this effort. The first was a fully dense Tungsten Carbide provided by Kennametal Inc. The other was extracted from an armor piercing (AP) projectile. The Kennametal Tungsten Carbide contains 5.7% Co, 1.9% Ta and less than 0.3% Nb and Ti. The reported Rockwell-A hardness is 93 and the static compressive strength is 58.2 GPa. The AP material contains 3-4% Ni, 0.4-0.8% Fe and 0.05-0.2% Co. The Rockwell-A hardness is 86-92. Static compressive strength for this material is 4.42 GPa and split cylinder test results provided a static tensile strength of 0.24-0.27 GPa. Properties for the two materials are provided in Table 1; c_l, c_s, and c_o are the longitudinal, shear, and bulk sound speeds, respectively.

Table 1: Elastic Properties for Tungsten Carbide

Material	Density (kg/m^3)	c_l (km/s)	c_s (km/s)	c_o (km/s)	Bulk Modulus (GPa)	Poisson's Ratio
Kennametal	14930	6.895	4.165	4.941	364.5	0.213
AP	14910	6.918	4.149	4.991	371.4	0.219

Samples of the AP material were prepared in the form of solid spheres and launched with a light-gas gun facility [3]. The test sphere strikes a thin plate of low-density non-metallic material and undergoes catastrophic fragmentation. Flash shadowgraphs are used to image the fragmented specimen at several stations. Only the ceramic debris appears on the shadowgraph because of the low density of the impact plate material. From the extent of fragmentation and velocity of debris expansion, fragmentation properties of the material can be inferred [4].

The experimental configuration for investigating the fragmentation properties of solids is shown in Figure 1. Spheres of the test material, mounted in lexan sabots, were launched at velocities between 2.44 to 3.43 km/s with a two-stage light-gas gun system. Tungsten Carbide spheres 6.45 ± 0.03 mm in diameter were used with a mass of 2.07 ± 0.01 grams. Fragment debris was diagnosed at two stations (approximately 80 mm and 250 mm) downstream from the input point. Two 150 kev flash x-ray tubes, placed approximately 400 mm from the line of debris travel, provided orthogonal shadow-graphs of the fragment debris, as shown in Figure 2. Appropriate delay times were calculated from the predicted impact velocity and the x-ray tubes were independently triggered from the second magnetic velocity coil. The fragment debris struck aluminum witness plates, which in some cases provided an independent measure of particle size and velocity statistics [3].

Three experiments were performed on the Tungsten Carbide ceramic, and in each test the impact velocity exceeded conditions needed to cause fragmentation in the test sample. For

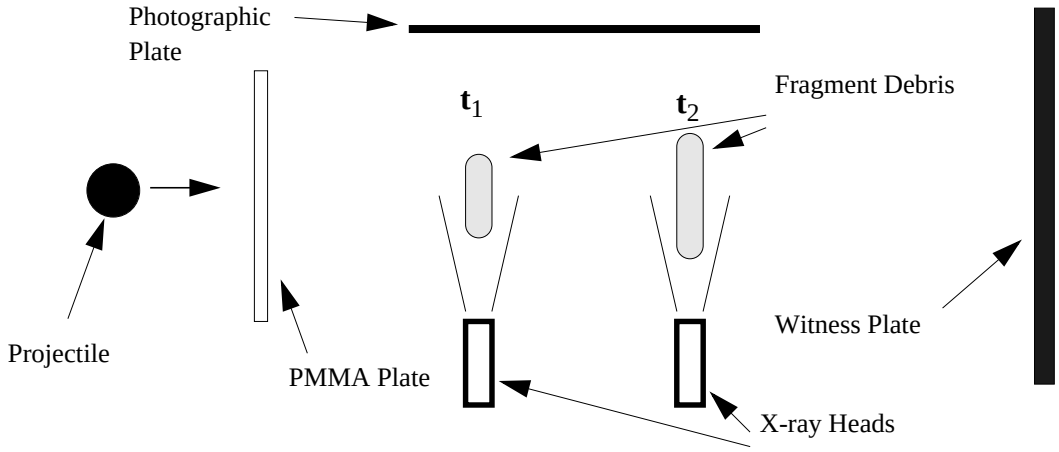

Figure 1. Experimental Configuration for Shadowgraphic and Witness Plate Diagnostic of Impact Fragmentation Experiments.

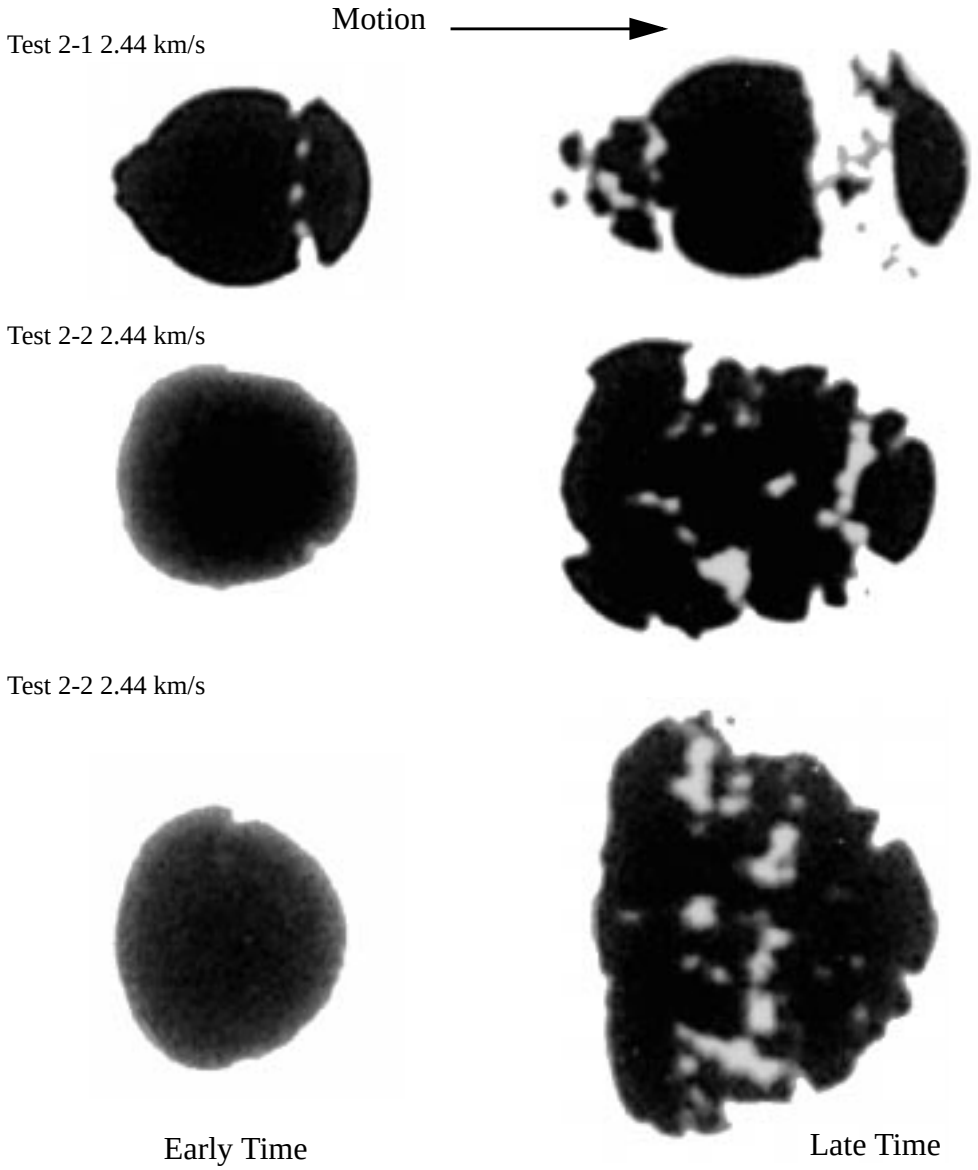

Figure 2. Shadowgraphic Images of Tungsten Carbide Fragment Debris.

each experiment, two images of the debris after impact with the PMMA plate are shown. The times after impact for each image are provided in Table 2. The velocity of the sample projectile prior to impact along with a nominal velocity of the fragment debris after impact, is also provided in Table 2. Axial and radial expansion velocities of the debris, which will be described shortly, complete the data in Table 2. A graphical display of the expansion data in Table 2 is given in Figure 3.

Test 2-1, with an impact velocity of 2.44 km/s, is just above the breakup threshold. Damage consists principally of spall segments separated from fore and aft regions of the spherical sample. There is also a slight increase in lateral diameter of the central section between the first and second X-ray, suggesting additional fragmentation or damage in this region also. In Tests 2-2 and 2-3, at systematically higher impact velocities, shock energy becomes more uniformly distributed, leading to more homogeneous fragmentation of the projectile. Shock energy imparted

Table 2: Test Data for Tungsten Carbide

Test	Impact Velocity (km/s)	X-Ray t_1 (μs)	X-Ray t_2 (μs)	Debris Velocity (km/s)	Radial Expansion Velocity (m/s)	Axial Expansion Velocity (m/s)
2-1	2.44	27.7	97.3	2.35	3 ±3	37 ±4
2-2	2.90	26.5	85.6	2.79	21 ±4	37±4
2.3	3.43	21.2	71.4	3.30	50 ±4	38 ±4

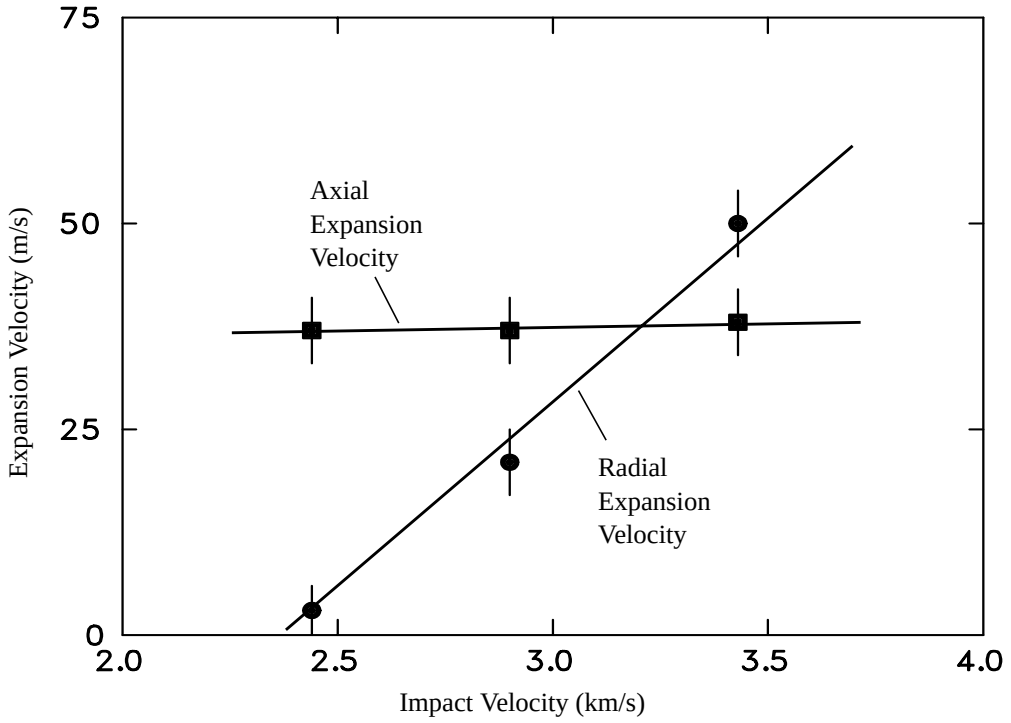

Figure 3. Fragment Debris Expansion Velocity for Tungsten Carbide Impacts.

to the test sphere is principally consumed in fragmentation of the body and in kinetic energy of the expanding debris. The latter energy is readily quantified through measurements of the

radial and axial expansion velocities of the fragment debris. Specifically, these velocities are determined from the ratio of the changes in half-diameter (radial velocity), or half-length (axial velocity), of the debris silhouette in the two shadowgraphs to the time between them.

It is of interest to note that the shock energy transferred into axial expansion energy of the fragment debris is independent of impact velocity over the test range whereas radial expansion increases markedly with impact velocity. The radial expansion velocity determines a breakup threshold at an impact velocity of approximately 2.4 km/s. The shock pressure of Tungsten Carbide on PMMA at this impact velocity is about 15 GPa.

The present experiments do not provide sensibly accurate measurements of the particle size created in the fragmentation event in that sufficient debris expansion was not allowed before shadowgraphic measurements were obtained. Nevertheless, applying the methods described in Grady and Kipp [4], which establish a characteristic size for the fragment debris from the shadowgraphic images and using a statistical method to account for fragment overlap, average fragment sizes of 1.1 mm, 0.8 mm and 0.7 mm were determined for the three tests.

COMPUTATIONAL COMPARISONS

Two series of CTH simulations were undertaken for this paper. The first simulation series used the P_{min} model for predicting fracture. The P_{min} model inserts the background material of CTH (referred to as void) into a computational cell when the cell pressure or principal stress exceeds (in tension) a time-independent criteria. This model has been successful in predicting hydrodynamic spall phenomena in many cases. One of the difficulties with the P_{min} model is that it has no memory. If a cell fails in tension and later experiences compression, the void will be removed and the code has no memory of the previous failure. Another difficulty is that a single criteria, such as P_{min}, cannot capture the complex time dependent phenomena of dynamic fracture and fragmentation. The second simulation series uses a more sophisticated model that includes both a memory (damage accumulation function) and a time dependent fracture initiation mechanism.

The new model is based on an energy-based spall and fragmentation theory of Grady and Kipp [2] and is implemented in CTH as follows. We form an integral of the material stress squared (σ^2) over time and compare that to a criteria (κ_G) determined from the fracture toughness. The integral is computed at all points within the material boundaries and advected over time with other computational variables. This integral should be recognized as a special case of the more general Tuler-Butcher failure criteria [6]. The integral is formed only when the material is in tension and is terminated after the first tensile wave turns to compression. A typical stress profile at some interior location is shown in Figure 4. The damage integral is coupled to the P_{min} model through a second function known as the "failed volume fraction, $\phi_f(t)$." The function ϕ_f ranges from 0 to 1 and is attached to or advected with the Grady-Kipp material. When the damage integral exceeds κ_G, ϕ_f is increased to one. The change in ϕ_f is made over ~10 time steps to minimize the potential for numerical difficulties in the Eulerian solution technique used by CTH. A time dependent void insertion criteria is formed from the P_{min} value and the failed volume fraction as $P_f(t) = P_{min}(1-\phi_f(t))$. The time dependent fracture criteria $P_f(t)$ is then used to insert void into failed cells that are in tension.

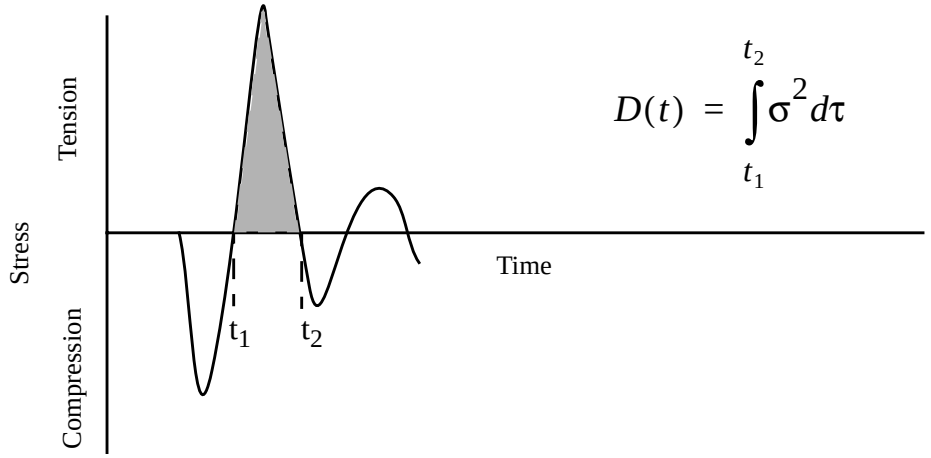

Figure 4. Typical Stress Wave Profile for Grady-Kipp Integration

The impacts described earlier were modelled using a two-dimensional cylindrical coordinate system to reduce computational overhead. As noted in the previous section, we expect a characteristic fragment size of ~1 mm. To represent the bulk of the fragment distribution, a cell size of 0.1 mm was chosen which allows us to distinguish fragments of ~0.2 mm in diameter. The computational zoning was square (0.1 x 0.1 mm) throughout the region the sphere traveled. After the projectile perforated the PMMA plate, all PMMA material was removed from the simulation and a velocity transformation was applied to reduce the movement of the debris through the mesh. The constitutive behavior and the equation of state of Tungsten Carbide was developed using wave profile data taken as a part of this study. Two wave profiles were fit to the constitutive model developed by Johnson and Cook [5]. A P_{min} value of 3.0 GPa was inferred from the dynamic spall data.

Figure 5 shows the results of three CTH simulations when the conventional P_{min} void insertion

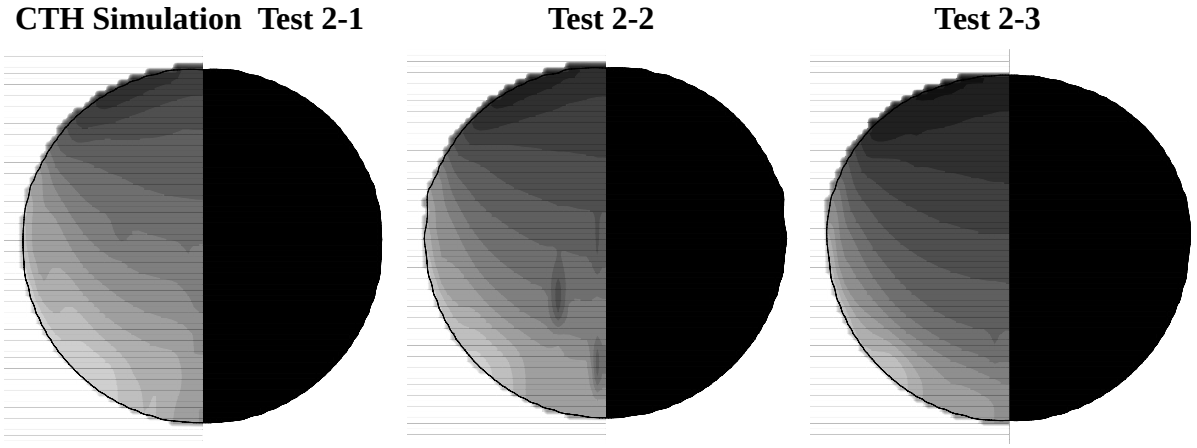

Figure 5. CTH Results with P_{min} Void Insertion Only.

model for fracture is applied. Each frame corresponds to one of the three impact velocities with the impact velocity increasing left to right with the direction of motion upwards. The time of each simulation corresponds to the earliest shadowgraph in Figure 2 (actual times are given in Table 2). The CTH images are reflected about the line of symmetry; the left side of each image displays a grey scale (black is 30 GPa and white is 1 GPa with a logarithmic spacing) in maxi-

mum tensile stress (over time) and the right side displays the material locations. The simulated peak tensile stress is 17 GPa, 21 GPa, 25 GPa for Tests 2-1, 2-2, and 2-3, respectively. For all three simulations, the peak tensile stress is greater than the P_{min} criteria of 3.0 GPa, although none of the images show any sign of discrete fractures. Some plastic deformation can be seen. The reason for the absence of fracture is the lack of memory or accumulated damage in the current P_{min} model. Careful inspection of the results indicated that void is inserted in various locations due to the initial tensile pulse but later compressive pulses remove the void from the simulation. The inability of this model to match the fragmentation patterns in Figure 2 is readily evident.

Figure 6 shows the results of three CTH simulations when the P_{min} model is coupled to the

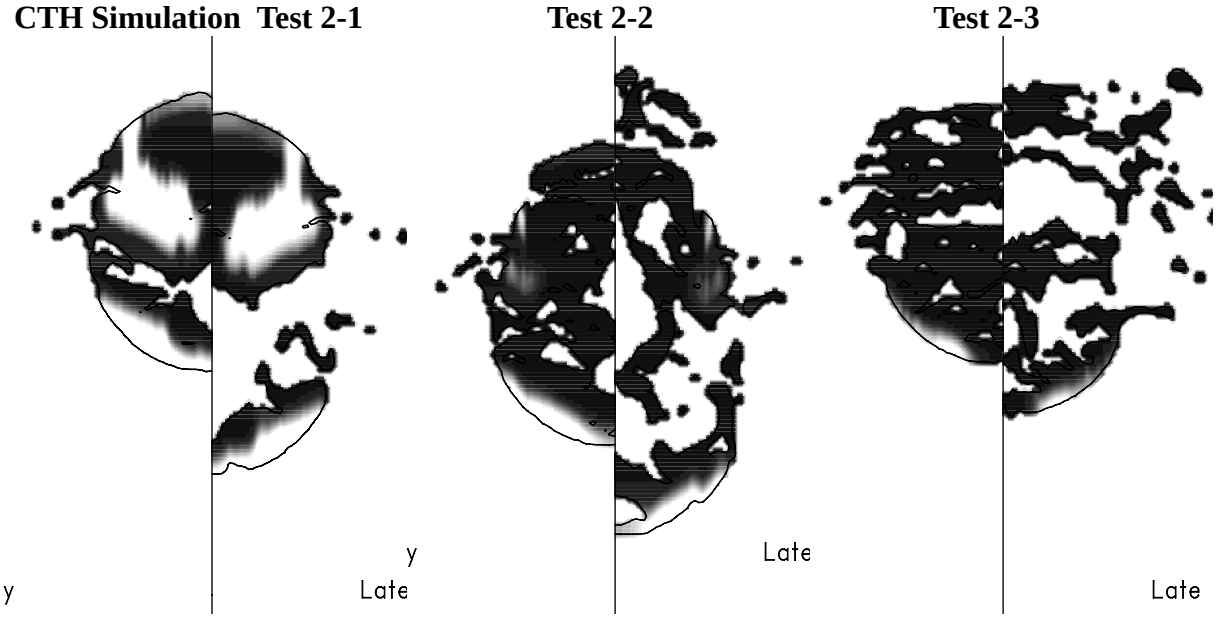

Figure 6. CTH Results with P_{min} Void Insertion Coupled to a Grady-Kipp Damage Integral.

Grady-Kipp damage integral as described above. The value of κ_G that was used (0.3 MPa^2 s) can be derived directly from the fracture toughness of Tungsten Carbide established from impact spall experiments [2]. Again, the impact velocity increases left to right. The CTH images are reflected about the line of symmetry with ϕ_f values displayed in a grey scale (black corresponds to fully failed and white to no failure). The left and right side of each CTH image correspond to the early and late shadowgraphs in Figure 2. The axial scale is shifted arbitrarily to place both snapshots in time at approximately the same location. A comparison between the computed and experimental expansion velocities is given in Table 3. The range in computed

Table 3: Experimental - Computational Expansion Velocity Comparison

Test	Measured Radial Expansion Velocity (m/s)	Computed Radial Expansion Velocity (m/s)	Measured Axial Expansion Velocity (m/s)	Computed Axial Expansion Velocity (m/s)
2-1	3 +/- 3	0	37 +/- 4	29

Table 3: Experimental - Computational Expansion Velocity Comparison

Test	Measured Radial Expansion Velocity (m/s)	Computed Radial Expansion Velocity (m/s)	Measured Axial Expansion Velocity (m/s)	Computed Axial Expansion Velocity (m/s)
2-2	21 +/- 4	17–20	37 +/- 4	39-73
2.3	50 +/- 4	30-43	38 +/- 4	42

velocities reflect the inclusion of the small fragments seen in all three simulations. The CTH simulations with the Grady-Kipp damage model show distinctly different features from the conventional P_{min} model. In Figure 6, an increase in the predicted damage as a function of impact velocity is evident. The general trend of increasing radial dispersion in the debris cloud is captured by the CTH simulations. Details of the distribution of debris fragments are not well characterized by the CTH simulations. In particular, the flattening of the rear surface of the projectile along with the retention of a spherical leading edge is missed almost entirely by the simulations. The simulations do not completely capture the constant axial expansion seen in the experiments, although, they do capture the increasing radial expansion as the impact velocity increases.

CONCLUSIONS

A series of experiments was conducted using spheres of Tungsten Carbide impacting PMMA plates over a range of velocities. At an impact velocity of 2.44 km/s damage consists principally of spall segments separated from fore and aft regions of the spherical sample. There was a slight increase in the lateral diameter of the central section between the first and second X-ray, suggesting additional fragmentation or damage in this region also. At high velocities, the shock energy was more uniformly distributed, leading to more homogeneous fragmentation processes. The shock energy imparted to the test sphere was consumed by fragmentation of the body and in kinetic energy of the expanding debris. The latter energy was quantified through measurements of the radial and axial expansion velocities of the debris. We noted that the shock energy transferred into axial expansion energy of the fragment debris was independent of impact velocity over the test range whereas radial expansion increases markedly with impact velocity. This series of well characterized experiments were used to assess the effectiveness of CTH in predicting the axial and radial dispersion of the projectile after break-up.

Current modelling capabilities in CTH reflect those in the shock physics community as a whole. Comparisons with the experimental data were made using the P_{min} model and an additional model founded on the energy-based theory of Grady and Kipp. We found that the simple P_{min} model was not capable of predicting the complex fragmentation behavior seen in the experiments, principally because of the lack of a memory or damage function. The CTH version of Grady-Kipp was capable of predicting the increase in radial expansion as the impact velocity increases but not the constant axial expansion with increasing impact velocity. We do not understand why the radial versus axial momentum partitioning is not being modelled correctly for this class of problems. One possibility for the differences is in the use of the two dimensional cylindrical geometry to model an inherently three dimensional phenomena. In the cylindrical geometry, each “fragment” is actually a ring. The ring has significantly different stress and fracture characteristics than would be expected for the same material in three dimen-

sional geometries.

We feel that the use of a physically based model, such as Grady-Kipp, is required to predict the complex fragmentation phenomena typical to high velocity impacts. We plan to continue our investigations of fragmentation phenomena with the computational framework developed for this paper.

REFERENCES

{1} McGlaun, J. M., S. L. Thompson, L. N. Kmetyk, and M. G. Elrick, *A Brief Description of the Three-Dimensional Shock Wave Physics Code CTH,* Sandia National Laboratories Report SAND89-0607, July (1990).

{2} Grady, D. E. and M. E. Kipp, *Dynamic Fracture and Fragmentation,* in High Pressure Shock Compression of Solids, J. R. Asay and M. Shahinpoor, editors, SpringerVerlag, 265 (1992).

{3} Grady, D. E. and M. E. Kipp, *Experimental Measurement of Dynamic Failure and Fragmentation Properties of Metals,* Int. J. Solids and Structures, (in press).

{4} Kipp, M. E., D. E. Grady, and J. W. Swegle, *Experimental and Numerical Studies of High-Velocity Impact Fragmentation,* Sandia National Laboratories Report SAND93-0773, August (1993).

{5} Johnson, G. R. and J. H. Cook, *Fracture Characteristics of Three Metals Subjected to Various Strains, Strain Rates, Temperatures, and Pressures,* Engrg. Frac. Mech., **21**, 31 (1985).

{6} Tuler, F. R. and B. M. Butcher, *A Criteria for the Time Dependence of Dynamic Fracture*, Int. J. Fract. Mech., **4**, 431 (1968).

This work was performed at Sandia National Laboratories supported by the U. S. Department of Energy under contract DE-AC04-94AL85000.